

explain the solid state effects shown by free base porphyrins is proposed, which takes into account possible rearrangements of porphyrin molecules in the crystal. Should these calculations give positive results, general conclusions could be drawn about porphyrin tautomerism.

The solid-state NMR results presented in this work do not appear to be in complete agreement with the previous X-ray analyses of the studied porphyrins. Although it is conceivable that the crystalline forms that we have employed for the CPMAS study are not the same as those used for the crystallographic analysis, it may be worthwhile to note that since hydrogen atoms are weak X-ray scatterers it is difficult to locate them by X-ray diffraction. This problem is highlighted when hydrogens are bonded to electronegative atoms like nitrogen, due to the distortion of the electron density along the N-H direction.⁶⁶ However, in the case of porphine (where $K = 1$) it is possible to reconcile the presence of the two tautomers in the solid with the localization of the central hydrogens proposed by the X-ray analysis, if it is assumed that the tautomeric process is coupled to a rotation of

the molecule as a whole in such a way that the translational symmetry of the crystal is maintained. This could be achieved by a rotation of 90° about the main molecular axis combined with the hydrogen migration process. We are currently studying this possibility using wide line spectroscopy. In any case, we have shown that ¹³C CPMAS NMR, when performed at different temperatures and corrected by intermolecular effects, is one of the most useful tools for studying dynamical processes in the solid state.

Acknowledgment. This research was supported by the National Institutes of Health under Grant GM 11973. Support by the Consejo Nacional de Investigaciones Cientificas y Tecnicas (CONICET) is also gratefully acknowledged. We thank Prof. David M. Grant and Charles L. Mayne (University of Utah) for help in recording the solution spectra within the frame of a NSF-CONICET binational grant. We are also grateful to Prof. Raymond J. Abraham (University of Liverpool) for discussions on ring current effects.

Registry No. TPrP, 22112-75-0; OEP, 2683-82-1; pyrrole, 109-97-7; butyraldehyde, 123-72-8.

(66) Taylor, R.; Kennard, O. *Acc. Chem. Res.* 1984, 17, 320.

Indirect Two-Dimensional Heteronuclear NMR Spectroscopy. (³¹P, ⁵⁷Fe) Spectra of Organoiron Complexes

Reinhard Benn,* Herbert Brenneke, Albert Frings, Herbert Lehmkuhl, Gerlinde Mehler, Anna Ruffńska, and Thomas Wildt

Contribution from the Max-Planck-Institut für Kohlenforschung, Kaiser-Wilhelm-Platz 1, D-4330 Mülheim a.d. Ruhr, Germany. Received December 14, 1987

Abstract: The indirect heteronuclear two-dimensional (2D) triple-resonance (S, I)-{¹H} NMR spectroscopy is introduced for measuring the chemical shift and scalar spin-spin coupling constants of an insensitive nucleus I via its scalar coupling $J(S, I)$ by detection of the nucleus S of higher sensitivity. The versatility of this approach is demonstrated by extracting $\delta(^{57}\text{Fe})$ and $J(\text{Fe}, \text{X})$ from (³¹P, ⁵⁷Fe)-{¹H} spectra of various dissolved $[(\eta^5\text{-Cp})(\text{L}_2)(\text{R})]\text{Fe}$, $[(\eta^3\text{-allyl})(\eta^5\text{-Cp})(\text{L})]\text{Fe}$, and $[(\eta^1, \eta^2\text{-alkenyl})(\eta^5\text{-Cp})(\text{L})]\text{Fe}$ complexes (R = alkyl, hydride; L = PR₃). In practice the sensitivity of 2D (³¹P, ⁵⁷Fe) spectra was found to be higher than that of the direct observation scheme by at least a factor $(\gamma_{\text{P}}/\gamma_{\text{Fe}})^{5/2}$. At 9.4 T typical recording times for 5-mm samples of low concentration (1-5%, v/v) are of the order of 1 h. Thus, the iron NMR parameters of many complexes become accessible in the most effective manner when the indirect (³¹P, ⁵⁷Fe) recording scheme is used. Due to the intrinsically higher resolving power of a two-dimensional experiment, small scalar couplings like ²J(Fe, F) and ¹J(Fe, H) were readily obtained from indirect two-dimensional spectra. Combinations of (¹H, ⁵⁷Fe) and (³¹P, ⁵⁷Fe) spectra yielded the relative signs of the $J(\text{Fe}, \text{X})$ couplings: ¹J(Fe, P) is positive and increases with increasing π -acceptor power of the phosphorus ligand L from 55 (L = PMe₃, R = H) to 149 Hz (L = PF₃). ¹J(Fe, H) is around +9 Hz (R = H), whereas ²J(P, H) in these complexes was found to be negative. In all of the allyl complexes investigated, ²J(Fe, F) (L = PF₃) is positive and around 3 Hz. In the quasi-tetragonal and -trigonal iron complexes, $\delta(^{57}\text{Fe})$ varies by about 4000 ppm. This can be rationalized qualitatively by the electronegativity of the atoms directly bonded to iron and the higher oxidation potential in the presence of more basic ligands L via the paramagnetic shielding term.

Complexes of iron play an important role in inorganic¹ and organometallic² chemistry as well in a variety of industrial processes³ and biological systems.⁴ The number of ⁵⁷Fe NMR studies of dissolved complexes,⁵ however, is still limited,⁶⁻⁸ and, conse-

quently, the total range of the ⁵⁷Fe shift scale is unknown. Only a few indirect scalar spin-spin couplings $J(\text{Fe}, \text{X})$ (e.g. X = ¹H,⁹ ¹³C,¹⁰ ¹⁵N,¹¹ and ³¹P^{7,9,10d,12}) have yet been reported. This is because the ⁵⁷Fe nucleus is one of the most insensitive nuclei in NMR spectroscopy, and the natural abundance of magnetically active iron is only 2.19%.⁶⁻⁸ Several approaches have been made to improve the recording conditions for this nucleus. Examples are steady-state pulse techniques,¹³ the use of high magnetic fields,

(1) Cotton, F. A.; Wilkinson, G. *Advanced Inorganic Chemistry*; Wiley: New York, 1980; p 765.

(2) Koerner von Gustorf, E. A.; Grevels, F.-W.; Fischler, T. *The Organic Chemistry of Iron*; Academic: New York, 1978, Vol. 1; 1981, Vol. 2. Wilkinson, G., Stone, F. G. A., Abel, E. W., Eds. *Comprehensive Organometallic Chemistry*; Pergamon: Oxford, 1982; Vol. 4, p 243; Vol. 8, p 939.

(3) Weissermel, K.; Arpe, H. J. *Industrielle Organische Chemie*; Verlag Chemie: Weinheim, FRG, 1978.

(4) Lee, H. C.; Gard, J. K.; Brown, T. L.; Oldfield, E. J. *J. Am. Chem. Soc.* 1985, 107, 4087; Nozawa, I.; Sato, M.; Hatano, M.; Kobayashi, N.; Osa, T. *Chem. Lett.* 1983, 1289.

(5) To the best of our knowledge, solid-state ⁵⁷Fe NMR studies have not been reported until now.

(6) Dechter, J. J. *Prog. Inorg. Chem.* 1985, 33, 393.

(7) Philipsborn, W. v. *Pure Appl. Chem.* 1986, 58, 513.

(8) Benn, R.; Ruffńska, A. *Angew. Chem.* 1986, 98, 851.

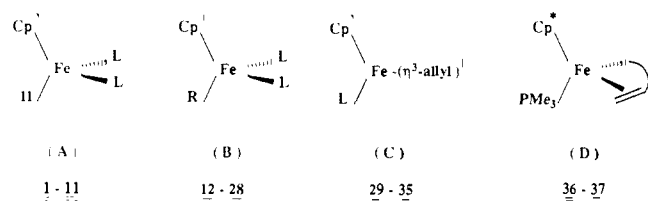
(9) Benn, R.; Brevard, C. *J. Am. Chem. Soc.* 1986, 108, 5622.

(10) (a) Koridze, A. A.; Petrovskii, P. V.; Gubin, S. P.; Fedin, E. I. *J. Organomet. Chem.* 1975, 93, C26. (b) Koridze, A. A.; Astakhova, N. M.; Petrovskii, P. V. *Izv. Akad. Nauk SSSR, Ser. Khim.* 1982, 956; 1982, 957. (c) Jenny, T.; Philipsborn, W. v.; Kronenbitter, J.; Schwenk, A. *J. Organomet. Chem.* 1981, 205, 211. (d) Mann, B. E. *J. Chem. Soc., Chem. Commun.* 1971, 1173.

(11) Morishima, I.; Inubushi, T. *J. Chem. Soc., Chem. Commun.* 1978, 106.

(12) Brevard, C.; Schimpf, R. *J. Magn. Reson.* 1982, 47, 528.

Chart I



which not only enhance the Boltzmann factor but also may shorten $T_1(\text{Fe})$ due to chemical shift anisotropy (CSA),¹⁴ and application of polarization transfer techniques like INEPT.¹² Each of these techniques has its own limitations. The sensitivity of the steady-state techniques is strongly influenced by $T_2(\text{Fe})$ and becomes more difficult when more than one line has to be recorded¹³ due to splittings of scalar couplings. Reasonable recording conditions for many iron compounds often are met only at 9.4–14 T, but such high-field spectrometers¹⁴ are not always available. The INEPT pulse scheme gives satisfactory results only if a good estimate for the ^{57}Fe shift can be made since pulse imperfections due to off-resonance effects can significantly diminish the enhancement by polarization transfer.^{15,16} Since the shift scales of the low- γ spin- $1/2$ metal nuclei may become extremely large, this can be a serious limiting condition.

In the following we introduce indirect two-dimensional heteronuclear double-quantum (S,I)- $\{^1\text{H}\}$ NMR spectroscopy, where S is a sensitive and I an insensitive nucleus.¹⁷ This approach circumvents all the above-mentioned problems and only requires that there is a nonzero scalar $J(\text{I,S})$ coupling with $J(\text{I,S}) > 1/T_2(\text{S})$. It is related to the experimentally less demanding indirect two-dimensional double-resonance ($^1\text{H,I}$) detection scheme,^{18,19} which has already been applied for recording ^{13}C ,²⁰ ^{15}N ,²¹ ^{113}Cd ,²² ^{183}W ,^{15,23} ^{103}Rh ,²⁴ ^{57}Fe ,⁹ and ^{187}Os ²⁵ NMR spectral parameters by detection of the protons and using the $J(^1\text{H,I})$ couplings. However, the only known $J(\text{H,Fe})$ coupling is a one-bond coupling, which is less than 10 Hz,⁹ and $^nJ(\text{H,Fe})$ couplings can be expected to be even smaller. On the other hand, phosphorus ligands are frequently present in iron complexes. The indirect two-dimensional ($^{31}\text{P},^{57}\text{Fe}$) spectroscopy would therefore seem to be promising, since the receptibility of the ^{31}P nucleus is high and the known $J(\text{Fe,P})$ couplings lie in the range between 15 and 60 Hz.^{7,9,12} In the

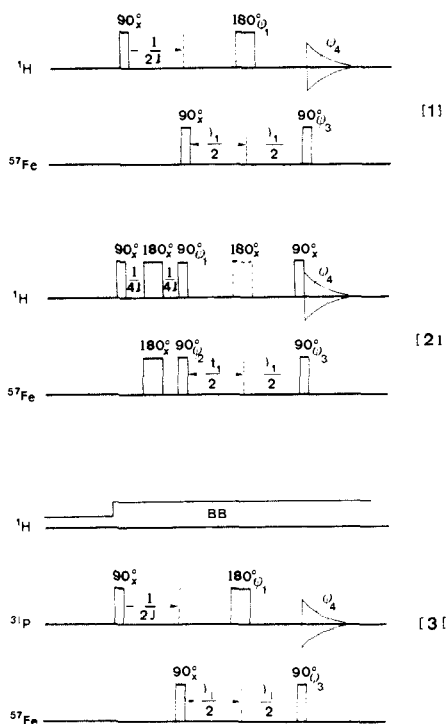


Figure 1. Pulsing schemes for the two-dimensional double-quantum spectroscopy. Sequences 1^{18c} and 2^{18b} were employed for ^1H detected double-quantum coherences of iron. $J = J(\text{Fe,H})$. 3 was used for the indirect heteronuclear ($^{31}\text{P},^{57}\text{Fe}$) spectroscopy, $J = J(\text{P,Fe})$. Inclusion of the dotted 180° proton pulse in sequence 2 eliminates the $J(\text{Fe,H})$ couplings from the F_1 dimension.

following, the versatility of this approach for the rapid detection of iron NMR parameters is described in detail. A variety of ^{57}Fe data with iron in various chemical environments is given, allowing a sound interpretation of factors governing $\delta(^{57}\text{Fe})$ and $J(^{57}\text{Fe,X})$. Furthermore, it is pointed out that suitable combinations of heteronuclear indirect two-dimensional (S,I)- $\{^1\text{H}\}$ NMR experiments can be used to determine the relative signs of the scalar couplings involved. Other extensions (e.g. multidimensional (S,I)- $\{^1\text{H}\}$ triple-resonance NMR spectroscopy) and applications of this approach are also feasible but will not be treated here in detail.

Experimental Section

Materials. The various types of iron complexes investigated here are illustrated in Chart I. Cp^* denotes a cyclic pentadienyl moiety, which is η^5 -bonded to iron. L symbolizes a phosphorus ligand. Bis(phosphine) complexes include those of chelating phosphines. In (B) R stands for η^1 -bonded organic ligands such as alkyl, vinyl, and alkenyl groups. The notation $(\eta^3\text{-allyl})'$ indicates that also alkyl-substituted η^3 -allyl moieties are taken into account. Depending on the stereochemical arrangement of the η^3 -allyl group, exo and endo isomers have to be considered. In group D, complexes with pentamethylcyclopentadienyl residues ($\eta^5\text{-Cp}^*$) and η^1, η^2 -bonded chelating organic ligands (36 and 37) and the complex $[(\eta^5\text{-Cp}^*)(\eta^2\text{-ethylene})(\text{hydrido})(\text{PMe}_3)]\text{Fe}$ (38) will be considered. The synthesis and some stability properties of all of these complexes are described in detail in ref 26–30. For the NMR measurements dilute (1–5%, v/v) samples dissolved in perdeuterated solvents such as toluene, benzene, and THF have been used.

NMR Measurements. Standard ^1H , $^{13}\text{C}\{^1\text{H}\}$, and $^{31}\text{P}\{^1\text{H}\}$ NMR spectral data of 1–38 are reported with discussion of the stereochemistry and the fluxionality of these compounds in ref 26–30. (For a recent detailed discussion of the dynamics of complexes of type B in solution

- (13) Schwenk, A. *Prog. Nucl. Magn. Reson. Spectrosc.* **1985**, *17*, 69.
 (14) Baltzer, L.; Becker, E. D.; Averill, B. A.; Hutchinson, J. M.; Gansow, O. A. *J. Am. Chem. Soc.* **1984**, *106*, 2444. Nozowa, T.; Hatano, M.; Sato, M.; Toida, Y.; Bartholdi, E. *Bull. Chem. Soc. Jpn.* **1983**, *56*, 3837. Lee, H. C.; Gard, J. K.; Brown, T. L.; Oldfield, E. *J. Am. Chem. Soc.* **1985**, *107*, 4087. Baltzer, L.; Becker, E. D.; Tschudin, R. G.; Gansow, O. A. *J. Am. Chem. Soc.* **1985**, *104*, 4040. Hafner, A.; Philipsborn, W. v.; Schwenk, A. *J. Magn. Reson.* **1987**, *74*, 433.
 (15) Benn, R.; Brenneke, H.; Heck, J.; Ruffińska, A. *Inorg. Chem.* **1987**, *26*, 2826.
 (16) Schenker, K. v.; Philipsborn, W. v. *J. Magn. Reson.* **1986**, *66*, 219.
 (17) For a time/frequency ($^{107}\text{Ag}/^{31}\text{P}$) experiment, cf.: Colquhoun, I. J.; McFarlane, W. *J. Chem. Soc., Chem. Commun.* **1980**, 145.
 (18) (a) Maudsley, A. A.; Müller, L.; Ernst, R. R. *J. Magn. Reson.* **1977**, *28*, 463. (b) Bodenhausen, G.; Ruben, D. *J. Chem. Phys. Lett.* **1980**, *69*, 185.
 (c) Bax, A.; Griffey, R. H.; Hawkins, B. L. *J. Magn. Reson.* **1983**, *55*, 301.
 (d) Bendall, M. R.; Pegg, D. T.; Doddrell, D. M. *J. Magn. Reson.* **1985**, *52*, 81. (e) Neuhaus, D.; Keeler, J.; Freeman, R. *J. Magn. Reson.* **1985**, *61*, 553.
 (19) For an improved pulse sequence for indirect two-dimensional double-resonance experiments, cf. Bax, A.; Subramanian, S. *J. Magn. Reson.* **1986**, *67*, 565.
 (20) Bax, A.; Summers, M. F. *J. Am. Chem. Soc.* **1986**, *108*, 2093. Bax, A.; Marzilli, L. G.; Summers, M. F. *J. Am. Chem. Soc.* **1987**, *109*, 566.
 (21) Sarka, S. K.; Glickson, J. D.; Bax, A. *J. Am. Chem. Soc.* **1986**, *108*, 6814. Mueller, L.; Schihnsnis, R. A.; Opella, S. J. *J. Magn. Reson.* **1986**, *66*, 379.
 (22) Frey, M. H.; Wagner, G.; Vašák, M.; Sørensen, O. W.; Neuhaus, D.; Wörgötter, E.; Kägi, J. H. R.; Ernst, R. R.; Wüthrich, K. *J. Am. Chem. Soc.* **1985**, *107*, 6847. Live, D.; Armitage, A.; Dalgarno, D. C.; Cowburn, D. J. *Am. Chem. Soc.* **1985**, *107*, 1175.
 (23) Benn, R.; Brevard, C.; Ruffińska, A.; Schroth, G. *Organometallics* **1987**, *6*, 938.
 (24) Benn, R.; Brenneke, H.; Ruffińska, A. *J. Organomet. Chem.* **1987**, *320*, 115.
 (25) Cabeza, J. A.; Mann, B. E.; Brevard, C.; Maitlis, P. M. *J. Chem. Soc., Chem. Commun.* **1985**, 65.

- (26) Lehmkuhl, H.; Mehler, G. *Chem. Ber.* **1985**, *118*, 2407.
 (27) Lehmkuhl, H.; Mehler, G.; Benn, R.; Ruffińska, A.; Schroth, G.; Krüger, C.; Raabe, E. *Chem. Ber.* **1987**, *120*, 1987, and references cited.
 (28) Wildt, T. Ph.D. Thesis, Universität Essen, 1987.
 (29) (a) Frings, A. Ph.D. Thesis, Ruhr Universität Bochum, 1988. (b) Frings, A.; Jonas, K., unpublished.
 (30) Green, M. L. H.; Wong, L.-L. *J. Chem. Soc., Dalton Trans.* **1987**, 411.

Table I. Phase Cycling in Sequences 1–3 Allowing Quadrature Detection in F_1 and F_2 Dimensions

scan	φ_1	φ_2	φ_3	φ_4
1–4	(X, X, X, X)		(X, -X, Y, -Y)	(X, -X, Y, -Y)
5–8	(-X, -X, -X, -X)		(X, -X, Y, -Y)	(X, -X, Y, -Y)
9–12	(Y, Y, Y, Y)		(X, -X, Y, -Y)	(X, -X, Y, -Y)
13–16 ^a	(-Y, -Y, -Y, -Y)		(X, -X, Y, -Y)	(X, -X, Y, -Y)
1–4	(Y, Y, Y, Y)	(X, -X, X, -X)	(X, X, Y, Y)	(X, -X, Y, -Y)
5–8 ^b	(-Y, -Y, -Y, -Y)	(-X, X, -X, X)	(X, X, Y, Y)	(X, -X, Y, -Y)

^aSequence 1 and 3. ^bSequence 2.

see ref 31 and 32. The fluxional behavior of dissolved **38** is described in ref 27). For **13**, **14**, **21**, and **28** the T_1 values were determined from $^{31}\text{P}\{^1\text{H}\}$ spectra at 310 K and 9.4 T by the inversion recovery technique.³³ From standard regression analysis the following phosphorus T_1 values were obtained: $T_1(\mathbf{13}) = 7.1 \pm 1.0$, $T_1(\mathbf{14}) = 8.1 \pm 1.0$, $T_1(\mathbf{21}) = 3.1 \pm 0.1$, and $T_1(\mathbf{28}) = 1.53 \pm 0.05$ s. All the indirect two-dimensional NMR spectra were run on a modified multinuclear Bruker WH 400 spectrometer, equipped with an ASPECT 2000 computer and a fast-pulse programmer (for details, see below) at constant temperature ($T = 300$ or 310 K) with a Bruker temperature controller.


Indirect 2D (^1H , ^{57}Fe) NMR Spectroscopy. The spectra were recorded with pulse sequences 1 and 2 illustrated in Figure 1. The experiments were performed on standard multinuclear Bruker spectrometers of the WH, and the WM series after slight hardware modifications. The ^1H pulses were generated via the decoupler channel. When quadrature detection was applied the offset for the proton, carrier frequency was set on the proton signal, which was coupled to the insensitive nucleus. The X frequency and 90° phase setting were generated with a PTS 160-MHz synthesizer normally used for X frequency generation in the direct observation scheme. The 180° phase shifts were performed with a B-SV 3 BX unit. However, as a result of the hardware modification only the X nuclei transmitter becomes activated while the receiver continues to be set up for proton observation. In this detection mode the X nucleus transmitter offset (01) and the ^1H decoupler offset (02) must be identical. The X nucleus carrier frequency can be placed in the middle of the desired frequency range of the insensitive nucleus by choosing the appropriate synthesizer frequency. When the commercially available multinuclear spectrometer equipment (10-W ^1H decoupler, 5-mm sample tubes inserted into a 10-mm multinuclear ^{31}P , ^{57}Fe probe head) is used, the 90° (^1H) pulses were 42 μs . The 90° (I) pulses in the low-frequency range (12–40 MHz) were between 40 and 50 μs .

Indirect 2D Heteronuclear (S,I)- $\{^1\text{H}\}$ NMR Spectroscopy. For a more versatile indirect observation scheme based on multiquantum coherences, a modified interface and a second PTS synthesizer for the X frequency generation were employed. Pulsing, phase cycling (cf. Table I), and observation of the I frequency are achieved via the standard multinuclear facilities of the spectrometer while pulsing or decoupling the second S frequency is carried out via the B-SV 3 unit. Generation of ^{31}P pulses via the second PTS 160 synthesizer is achieved via frequency doubling. The power level of the ^1H decoupler can be varied and mode switched between CW and BB under computer control. This hardware configuration allows experiments using sequence 3 to be carried out in addition to pulse sequences 1 and 2. Other experimental procedures such as multinuclear polarization transfer or NOE experiments are also feasible.

In order to take advantage of all these pulsing facilities, a special tunable probe head was employed. For these experiments a 5-mm probe head with temperature control was used. It is supplied with a deuterium lock channel, a doubly tuned inner coil for ^1H and ^{31}P and an outer coil for the low- γ I nuclei. This coil is tunable in the frequency range from 9 to 41 MHz. Spin $1/2$ nuclei like ^{187}Os , ^{57}Fe , ^{103}Rh , ^{183}W , and ^{15}N as well as insensitive quadrupolar nuclei like ^{61}Ni or ^{99}Ru can be observed in the indirect detection mode via ^{31}P or ^1H . In our experiments the 90° pulses were 8 μs (^1H), 28 μs (^{31}P), and from around 30 μs (^{57}Fe) (12.9 MHz) to around 15 μs (^{15}N) (40.5 MHz) in the I frequency range, respectively. Pulse sequences 1–3 (sequence 2 with a 180° proton pulse in the evolution period) yield in F_1 dimension the chemical shift of the insensitive nucleus $\delta(\text{I})$ and its scalar couplings with heteronuclei $J(\text{I},\text{X})$. Elimination of the second dotted proton 180° pulse in sequence 2 yields the $J(\text{I},\text{S})$ coupling in both the F_2 and the F_1 dimensions. Typical acquisition parameters using sequences 1–3 require a preparation time of around 2s. The number of transitions for each t_1 increment varied be-

Table II. ^{57}Fe NMR Parameters of $[(\eta^5\text{-Cp})(\text{hydrido})(\text{PR}_3)_2]\text{Fe}$ Complexes ($T = 300$ K Except for **1**, **3–7**, and **9** Where $T = 310$ K)

$\eta^5\text{-Cp}'$	$(\text{PR}_3)_2$	no.	$\delta(^{57}\text{Fe})$	$J(\text{Fe},\text{P})$
C_5H_5	$(\text{PMe}_3)_2$	1	1309 ^a	59.0
C_5H_5	$(\text{PMe}(\text{C}_6\text{H}_5)_2)_2$	2	1354	61.0
C_5H_5	$(\text{P}(\text{C}_6\text{H}_5)_3)_2$	3	1564	61.0
C_5H_5	$(\text{C}_6\text{H}_5)_2\text{P}(\text{CH}_2)_2\text{P}(\text{C}_6\text{H}_5)_2$	4	823	62.0
MeC_5H_4	$(\text{C}_6\text{H}_5)_2\text{P}(\text{CH}_2)_2\text{P}(\text{C}_6\text{H}_5)_2$	5	868	62.0
C_5H_5	$(\text{C}_6\text{H}_5)_2\text{P}(\text{CH}_2)_4\text{P}(\text{C}_6\text{H}_5)_2$	6	1452	61.0
C_5H_5	$(i\text{-Pr})_2\text{P}(\text{CH}_2)_3\text{P}(i\text{-Pr})_2$	7	1089	58.0
indenyl	$(i\text{-Pr})_2\text{P}(\text{CH}_2)_3\text{P}(i\text{-Pr})_2$	8	1825	60.0
C_6H_7^b	$(i\text{-Pr})_2\text{P}(\text{CH}_2)_3\text{P}(i\text{-Pr})_2$	9	1659	50.0
C_6H_7^b	$(i\text{-Pr})_2\text{P}(\text{CH}_2)_2\text{P}(i\text{-Pr})_2$	10	1225	58.0
EtC_6H_6^c	$(i\text{-Pr})_2\text{P}(\text{CH}_2)_2\text{P}(i\text{-Pr})_2$	11	1233	52.0

^aAt $T = 300$ K; $\delta(^{57}\text{Fe}) = 1294$. ^b $\text{C}_6\text{H}_7 =$ . ^c $\text{EtC}_6\text{H}_6 =$



tween 32 and 320 scans. Between 15 and 256 data points were chosen for generation of the F_1 dimension, and for the spectral range of the insensitive iron nucleus a spectral width up to 50000 Hz was covered within one experiment. In practice it posed no difficulties to identify the cross peaks even if the corresponding iron shifts were 25 kHz apart from the chosen carrier frequency in F_1 dimension (c.f. also ref 15). Sequences 1 and 3 were employed mostly when large spectral widths had to be covered for the detection of the unknown $\delta(\text{I})$ shifts since they contain fewer pulses. Generally, a second experiment with a reduced spectral width of 1000 or 500 Hz was carried out to check that the observed signals were not folded in F_1 dimension and in order to determine $\delta(\text{I})$ more exactly. The two-dimensional spectra were subjected to sine bell and shifted sine bell apodization functions in both dimensions, and zero-filling in the F_1 dimension was employed before Fourier transformation. All spectra are presented in the magnitude mode. For checking the efficiency of the indirect observation scheme, the iron spectrum of **30** was also directly recorded. For this purpose a 10-mm sample tube containing a solution of identical concentration was measured in a 10-mm probe head optimized for direct detection of low- γ nuclei (the 90° pulse of this probe head was 40 μs). The ^1H and ^{31}P chemical shifts are reported as δ values relative to external Me_4Si and 85% H_3PO_4 , respectively. The ^{57}Fe shifts were calculated via their absolute frequencies with the conversion factor: 12.975 570 MHz corresponds to $\delta(^{57}\text{Fe}) = 1532$ for ferrocene, while $\delta(^{57}\text{Fe}(\text{CO})_5) = 0$.³⁴ Typical error limits for the iron shifts as obtained from the two-dimensional spectra are between 1 and 2 ppm. For the $J(\text{P},\text{Fe})$ and $J(\text{H},\text{Fe})$ couplings the error limits are smaller than 1.5 and 0.5 Hz, respectively.

Results

^{57}Fe NMR parameters of hydridoiron complexes are listed in Table II. The data of complexes **2**, **7**, **8**, **10**, and **11** were obtained from proton-decoupled two-dimensional ^{31}P -detected (^{31}P , ^{57}Fe) spectra (see sequence 3 in Figure 1), while for the complexes **1**, **3–7** and **9** ^1H -detected double-quantum spectroscopy (sequence 1 in Figure 1) was employed. When the latter techniques is used, $\delta(^1\text{H})$, $J(\text{Fe},\text{H})$, and $J(\text{P},\text{H})$ can be obtained from the F_2 dimension whereas $\delta(^{57}\text{Fe})$ and $J(\text{P},\text{Fe})$ (even though the ^{31}P nuclei were not excited in this experiment) can be derived from the F_1 dimension. Exact values for $J(\text{Fe},\text{P})$ are more readily obtained from one-dimensional ^{31}P -detected double-quantum spectroscopy (setting $t_1 = 0$ in sequence 3) since in the former experiments long recording times are required for high digital resolution in the F_1 dimension. For all phosphorus ligands, the high-frequency proton cross peak correlates with the low-frequency iron peak in all 2D ($^1\text{H},\text{Fe}$) spectra (cf. Figure 2). Since the phosphorus nuclei were not excited, it follows that the sign of $^1J(\text{Fe},\text{P})$ is opposite the sign of $^2J(\text{P},\text{H})$. By the same argument, it follows from a 2D ($^{31}\text{P},\text{Fe}$) spectrum of **1** with CW decoupling of the PMe_3 protons that the sign of $^1J(\text{Fe},\text{H})$ is opposite the sign of $^2J(\text{P},\text{H})$. Both types of experiments therefore yield $\text{sign } ^1J(\text{P},\text{Fe}) = \text{sign of } ^1J(\text{H},\text{Fe})$ (cf. Figure 2).

The ^{57}Fe NMR parameters of the complexes **12–28**, which were obtained with sequence 3 (cf. Figure 1), are listed in Table III.

(31) Blackburn, B. K.; Davies, S. G.; Whittaker, M. *J. Chem. Soc., Chem. Commun.* **1987**, 1344. Johnston, P.; Loonat, M. S.; Ingham, W. L.; Carlton, L.; Covielle, N. *J. Organometallics* **1987**, 6, 211.

(32) Davies, S. G. Dordor-Hedgecock, I. M.; Sutton, K. H.; Whittaker, M. *J. Am. Chem. Soc.* **1987**, 109, 5711.

(33) Martin, M. L.; Martin, G. J.; Delpuech, J. J. *Practical NMR Spectroscopy*; Heyden: London, 1980; p 254 f.

(34) For $\delta(^{57}\text{Fe})$ of $\text{Fe}(\text{CO})_5$ and $(\eta^5\text{-Cp})_2\text{Fe}$, cf.: ref 10c and Haslinger, E.; Robien, W.; Schögl, K.; Weissensteiner, W. *J. Organomet. Chem.* **1981**, 218, C11.

Table III. ^{57}Fe NMR Parameters of $[(\eta^5\text{-Cp}')(\text{R})(\text{PR}_3)_2]\text{Fe}$ Complexes at $T = 300\text{ K}$

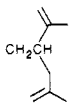
$\eta^5\text{-Cp}'$	$(\text{PR}_3)_2$	R	no.	$\delta(^{57}\text{Fe})$	$^1J(\text{P,Fe})$
C_5H_5	$(\text{PMe}_3)_2$	J	12	4287	60
C_5H_5	$(\text{PMe}_3)_2$	Me	13	2342	61
MeC_5H_4	$(\text{PMe}_3)_2$	Me	14	2318	61
Me_2C_5	$(\text{PMe}_3)_2$	Me	15	2679	60
C_5H_5	$(\text{PMe}(\text{C}_6\text{H}_5)_2)_2$	Me	16	2427	61
MeC_5H_4	$(\text{PMe}(\text{C}_6\text{H}_5)_2)_2$	Me	17	2451	61
C_5H_5	$(\text{C}_6\text{H}_5)_2\text{P}(\text{CH}_2)_2\text{P}(\text{C}_6\text{H}_5)_2$	Me	18	1833	60
C_5H_5	$(\text{PMe}_2(\text{C}_6\text{H}_5))_2$	Et	19	2487	63
MeC_5H_4	$(\text{PMe}_2(\text{C}_6\text{H}_5))_2$	Et	20	2542	62
C_5H_5	$(i\text{-Pr})_2\text{P}(\text{CH}_2)_3\text{P}(i\text{-Pr})_2$	Et	21	2999	59
C_5H_5	$(\text{PMe}_3)_2$	$\text{CH}=\text{CH}_2$	22	2350	60
C_5H_5	$(\text{PMe}(\text{C}_6\text{H}_5)_2)_2$	$\text{CH}=\text{CH}_2$	23	2524	61
C_5H_5	$(\text{C}_6\text{H}_5)_2\text{P}(\text{CH}_2)_2\text{P}(\text{C}_6\text{H}_5)_2$	$\text{CH}=\text{CH}_2$	24	1807	60
C_5H_5	$(\text{P}(\text{OMe})_3)_2$	$\text{CH}_2\text{CH}=\text{CH}_2$	25	1691	102
C_5H_5	$(\text{P}(\text{OMe})_3)_2$	$\text{CH}_2\text{CMe}=\text{CH}_2$	26	1744	102
C_5H_5	$(\text{P}(\text{OMe})_3)_2$		27	1608	103
C_5H_5	$(\text{PF}_3)_2$	$\text{CH}_2\text{CH}=\text{CH}_2$	28	594	127

Table IV. ^{57}Fe NMR Parameters of *exo*- $[(\eta^3\text{-Allyl})(\eta^5\text{-Cp}')(\text{PR}_3)]\text{Fe}$ Complexes at $T = 300\text{ K}$

$\eta^5\text{-Cp}'$	PR_3	$\eta^3\text{-allyl}'$	no.	$\delta(^{57}\text{Fe})$	$J(\text{P,Fe})$
Me_2C_5	PMe_3	$\eta^3\text{-CH}_2\text{CHCH}_2$	29	2246	70
C_5H_5	PF_3	$\eta^3\text{-CH}_2\text{CHCH}_2$	30	997	147 ^a
C_5H_5	$\text{P}(\text{OMe})_3$	$\eta^3\text{-CH}_2\text{CMeCH}_2$	31	1667	108
C_5H_5	$\text{P}(\text{OMe})_3$	$\eta^3\text{-syn-CH}_2\text{CHCHMe}$	32	1622	111
C_5H_5	PF_3	$\eta^3\text{-syn-CH}_2\text{CHCHMe}$	33	1039	149 ^a
C_5H_5	PF_3	$\eta^3\text{-syn-CH}_2\text{CHCHMe}^b$	34	906	145 ^a
C_5H_5	$\text{P}(\text{OC}_6\text{H}_5)_2\text{-menthyl}$	$\eta^3\text{-CH}_2\text{CMeCH}_2$	35	1871	93

^a $^2J(\text{Fe,F})$ around +3 Hz. ^bEndo isomer.

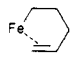
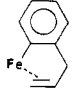
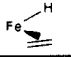
When PF_3 ligands are present, more complex spin systems for the $(\text{PF}_3)_2\text{Fe}$ moiety result; e.g., **28** gives rise to an $\{\text{AA}'\text{M}_3\text{M}_3'\text{X}\}$ spin system ($\text{A} = ^{31}\text{P}$, $\text{M} = ^{19}\text{F}$, $\text{X} = ^{57}\text{Fe}$). In Figure 3 the spectrum obtained via the indirect two-dimensional (^{31}P ,Fe) technique is compared to the conventional one-dimensional $^{31}\text{P}\{^1\text{H}\}$ spectrum (A part) of the $\{\text{AA}'\text{M}_3\text{M}_3'\}$ spectrum. Both types of experiments yield $^2J(\text{P,P}') = -179.1\text{ Hz}$, $^1J(\text{P,F}) = -1297.5$ and $^3J(\text{F,P}) = -7.2$, $^4J(\text{F,F}) = 0$. In addition, $J(\text{Fe,P}) = 126.7\text{ Hz}$ was derived from the two-dimensional indirect spectrum. Analysis of the ABX spin system ($\text{A}, \text{B} = ^{31}\text{P}$, $\text{X} = ^{57}\text{Fe}$) of **27** yielded $^2J(\text{P}_\text{A},\text{P}_\text{B}) = -159.4\text{ Hz}$ and $^1J(\text{P}_\text{A},\text{Fe}) = ^1J(\text{P}_\text{B},\text{Fe}) = 102.5\text{ Hz}$.

In Table IV $\delta(^{57}\text{Fe})$ and $J(\text{Fe,P})$ of $[(\eta^3\text{-allyl})(\eta^5\text{-Cp}')\text{PR}_3]\text{Fe}$ complexes are listed. The ^{57}Fe chemical shift is strongly influenced by the type of phosphorus ligand. As observed for the $[(\eta^5\text{-Cp}')(\text{PR}_3)_2(\text{R})]\text{Fe}$ complexes, the shielding of the iron nucleus increases when ligands acting as strong π -acceptors (soft Pearson bases) are present.

The stereochemistry of the allyl groups in these type of complexes can be derived³⁵ from $J(\text{P,C})$ and $J(\text{P,H})$. $\delta(^{57}\text{Fe})$ of the *exo* and *endo* isomers **33** and **34** differs by more than 130 ppm. ($\delta(^{31}\text{P})$ of **33** and **34** differs by 8.1 ppm). In the reverse proton-decoupled two-dimensional (^{31}P , ^{57}Fe) spectrum of the more stable *exo* isomer, a long-range $^2J(\text{Fe,F})$ coupling was resolved (c.f. Figure 4). Since the ^{19}F nucleus was not excited and since the low-frequency ^{31}P peak correlates with the high-frequency ^{57}Fe peak, it follows that the sign of $^2J(\text{Fe,F})$ is opposite the sign of $^1J(\text{P,F})$.

The ^{57}Fe NMR data of the complexes **36** and **37** in which alkenyl rests are η^1,η^2 -bonded to an $[(\text{Cp}^*)(\text{PMe}_3)]\text{Fe}$ fragment are similar to those obtained for $[(\text{Cp}^*)(\text{Me})(\text{PMe}_3)_2]\text{Fe}$ (**15**) (cf. Table V). If the σ -bonded carbon atom is replaced by a hydrogen atom (**38**), the shielding of the iron nucleus is enhanced. A similar

Table V. ^{57}Fe NMR Parameters of $[(\eta^5\text{-Cp}^*)(\text{PMe}_3)(\text{organyl})]\text{Fe}$ Complexes at $T = 300\text{ K}$

iron organyl rest	no.	$\delta(^{57}\text{Fe})$	$J(\text{Fe,P})$
	36	2896	59
	37	2997	53
	38	1480	55

observation is made for the $[(\eta^5\text{-Cp}')(\text{R})(\text{PR}_3)_2]\text{Fe}$ complexes; e.g. compare $\delta(^{57}\text{Fe})$ of **1** ($\text{R} = \text{H}$) with **13** ($\text{R} = \text{Me}$).

Discussion

Sensitivity Considerations. In Figure 5 the conventional one-dimensional ^{57}Fe spectrum of **30** is compared with its two-dimensional phosphorus-detected double-quantum ^{57}Fe spectrum. For the former experiment a 10-mm sample tube was employed. A total of 69 000 scans were accumulated, yielding a signal to noise ratio for the iron-phosphorus doublet of about 5 after 66 h. The indirect two-dimensional proton-decoupled (^{31}P , ^{57}Fe) spectrum was recorded with a 5-mm sample containing a solution with a concentration identical with that of the 10-mm sample. $\delta(^{57}\text{Fe})$ results from the position of the cross peaks in F_1 dimension whereas $J(\text{Fe,P})$ and $J(\text{P,F})$ are displaced in the F_2 projection. The signal to noise ratio of the highest peak in this projection was around 90 after recording for 8 h. Taking into account the 18-fold higher S/N value, the 8-fold shorter recording time, the filling factor of 4, and the higher multiplicity of the indirect detected signal, the indirect detection scheme is about 600 times more sensitive.³⁶ The gain in sensitivity for indirect detection of double-quantum coherences relative to direct observation is $(\gamma_\text{P}/\gamma_\text{Fe})^{5/2}$ or even $(\gamma_\text{P}/\gamma_\text{Fe})^3$ when radio frequency noise contributions are neglected. Thus, the enhancement factor achieved experimentally corresponds closely to that which is theoretically expected.

In the calculation given above, we neglected the fact that the repetition time for the direct acquisition is governed by T_1 of the insensitive iron nucleus, which often is significantly longer than T_1 of the sensitive phosphorus nucleus. This is because the $T_1(^{31}\text{P})$

(35) For typical $^3J(\text{P,H})$ and $^2J(\text{P,C})$ values in $(\eta^5\text{-Cp})\text{PR}_3\text{M}$ complexes ($\text{M} = \text{Ru, Fe}$), cf.: ref 26 or Lehmkuhl, H.; Mauermann, H.; Benn, R. *Justus Liebig's Ann. Chem.* **1980**, 754 and Benn, R.; Schroth, G. *Org. Magn. Reson.* **1980**, 14, 435.

(36) The actual sensitivity was calculated from $(\text{S/N})(\text{time})^{-1/2}nm$, where S/N is the signal to noise ratio of the F_2 projection, "time" denotes the overall spectral recording time, n symbolizes the number of molecules in the sample tube (filling factor), and m is a factor due to those multiplet splittings in the F_2 dimension, which are not available when the direct recording scheme is employed. (e.g. for **30**: $m = 8/3$ since the quartet due to $^1J(\text{P,F})$ is only observable in the indirect detection scheme).

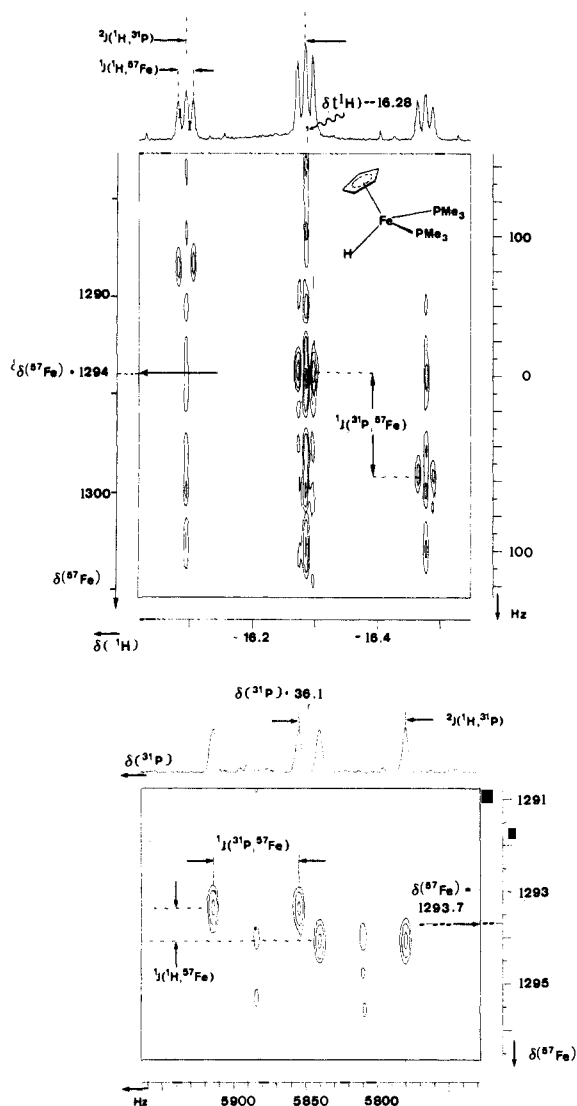


Figure 2. Indirect two-dimensional NMR spectrum of $[(\eta^5\text{-Cp})(\text{PMe}_3)_2\text{Fe}]$ (**1**) at $T = 300$ K: (a) $(^1\text{H}, ^{57}\text{Fe})$ spectrum and (b) $(^{31}\text{P}, ^{57}\text{Fe})$ spectrum with CW decoupling of the methyl protons. Spectrum a yields $\delta(^{57}\text{Fe})$ and $^1J(\text{P}, \text{Fe})$ in the F_1 dimension and $\delta(^1\text{H})$, $^1J(\text{H}, \text{Fe})$, and $^2J(\text{H}, \text{P})$ in the F_2 dimension. In spectrum b from the F_1 dimension $\delta(^{57}\text{Fe})$ and $J(\text{H}, \text{Fe})$ are obtained, whereas from the F_2 dimension $\delta(^{31}\text{P})$, $^1J(\text{P}, \text{Fe})$, and $^2J(\text{P}, \text{H})$ are obtained. From the positions of the cross peaks in both contour plots it follows that $^1J(\text{Fe}, \text{P})$ and $^1J(\text{Fe}, \text{H})$ are positive, whereas $^2J(\text{P}, \text{H})$ is negative. This figure demonstrates the high resolving power of the two-dimensional experiment since $J(\text{Fe}, \text{H})$ can be obtained more easily from the contour plot b than from the projection of spectrum a.

values of complexes are often significantly shorter than those of the uncomplexed ligands.³⁷ In fact the $T_1(^{31}\text{P})$ values for e.g. **13**, **14**, **21**, and **28** are only some seconds (c.f. the Experimental Section). Moreover, we found that in the most cases relatively short recycle times (ca. 3 s) can be used. This may cause an uncomplete suppression of the parent signal, which, however, can be tolerated if $J(\text{Fe}, \text{P})$ is not too small (compared to $W_{1/2}(^{31}\text{P})$). If necessary a special pulse sequence¹⁹ can be applied for an optimum suppression of parent signals. When polarization transfer schemes like INEPT or DEPT³⁸ are employed, the repetition time for both the direct and indirect observation scheme is determined

(37) Pregosin, P. S. In *Methods in Stereochemical Analysis*; Verkade, J. G., Quin, L. D., Eds.; Verlag Chemie: Weinheim, FRG, 1987; Vol. 8, p 466 f.

(38) Morris, G. A. L. Freeman, R. J. *Am. Chem. Soc.* **1979**, *101*, 760. Doddrell, D. M.; Pegg, D. T.; Bendall, M. R. *J. Magn. Reson.* **1982**, *48*, 323. For a review, cf.: Benn, R.; Günther, H. *Angew. Chem.* **1983**, *95*, 381 or Derome, A. E. *Modern NMR Techniques for Chemistry Research*; Pergamon: New York, 1987.

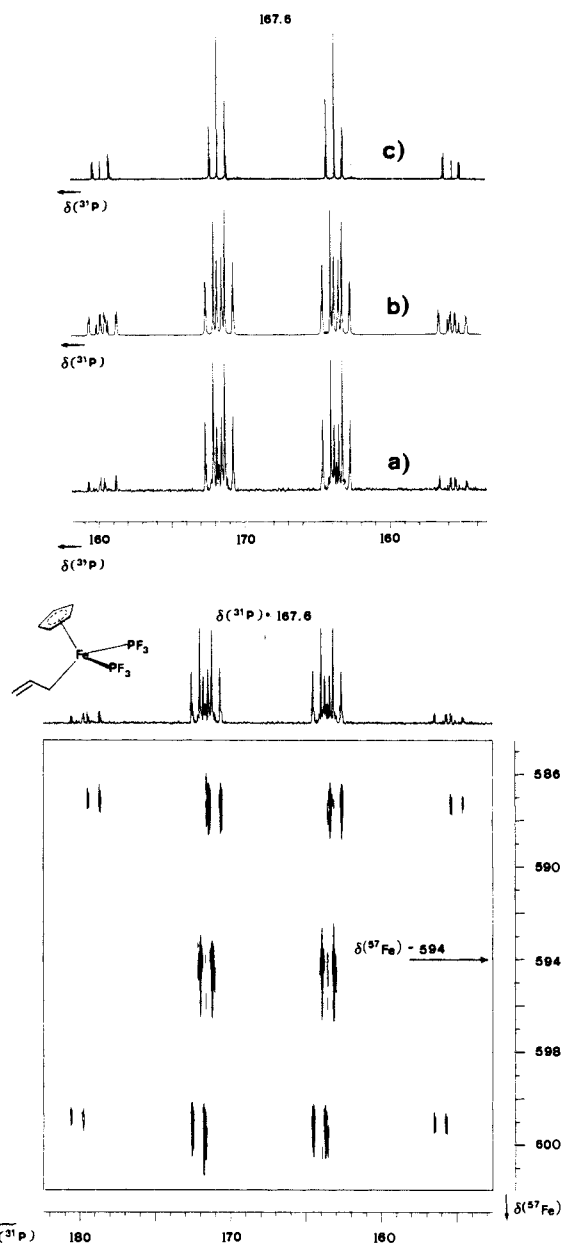


Figure 3. Contour plot of the indirect two-dimensional (F_1, F_2) proton-decoupled spectrum of $[(\eta^5\text{-Cp})(\eta^1\text{-CH}_2\text{CHCH}_2)(\text{PF}_3)_2\text{Fe}]$ (**28**). In trace a the F_2 projection stemming from the two-dimensional spectrum is presented. b shows the X part of the simulated $\{\text{AA}'\text{M}_3\text{M}_1'\text{X}\}$ spin system ($\text{A} = ^{31}\text{P}$, $\text{M} = ^{19}\text{F}$, $\text{X} = ^{57}\text{Fe}$). Note that the difference between trace b and a is due to the imperfect suppression of signals resulting from the isotomer with magnetically inactive iron. In trace c the conventional 162-MHz $^{31}\text{P}\{^1\text{H}\}$ spectrum of **28** is presented.

by $T_1(^{31}\text{P})$ and the latter experiment can be expected to be more sensitive by a factor of about $(\gamma_{\text{P}}/\gamma_{\text{Fe}})^2$. In practice, however, this factor can be exceeded because the indirect observation scheme is less prone to missetting of the carrier frequency than the polarization transfer techniques¹⁵ (cf. also the Experimental Section).

The resolving power of a two-dimensional experiment is at least as great as that of its corresponding one-dimensional analogue and usually greater. As a result, small couplings can be observed more easily. As shown explicitly in Figure 4, the magnitude and the relative sign of $J(\text{Fe}, \text{F})$ in **30** was obtained from the positions of the cross peaks in Figure 5 (cf. Table IV). The high resolving power of the indirect detection scheme in resolving $^1J(\text{Fe}, \text{H})$ is evident in Figure 2. Additionally, the indirect two-dimensional technique is much more sensitive, allowing apodization functions,³⁹

(39) Lindon, J. C.; Ferrige, A. G. *Prog. Nucl. Magn. Reson. Spectrosc.* **1980**, *14*, 27.

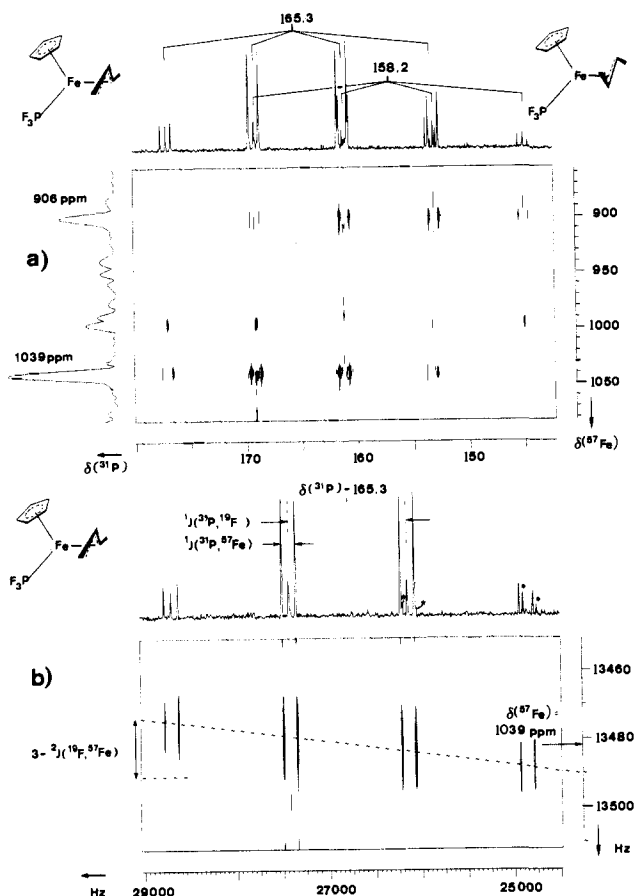
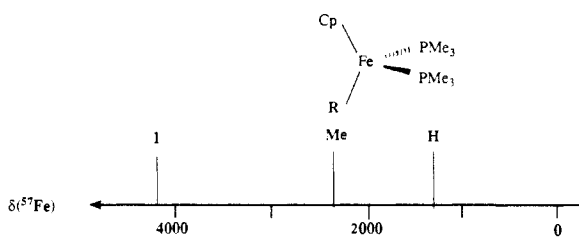


Figure 4. Contour plot a and its expansion b of the indirect two-dimensional (F_1, F_2) proton-decoupled ($^{31}\text{P}, ^{57}\text{Fe}$) spectrum of the *exo*-(**33**) and *endo*-(**34**) isomers of $[(\eta^5\text{-Cp})(\eta^3\text{-1-syn-methylallyl})(\text{PF}_3)]\text{Fe}$. $\delta(^{57}\text{Fe})$ of both isomers can be obtained from the F_1 projection. The expansion of the range containing the cross signals of the major isomer b shows that there is a $^2J(\text{F}, \text{Fe})$ coupling, which is of opposite relative sign to $J(\text{P}, \text{F})$. In the F_2 projection of b the lines belonging to the minor isomers are marked by asterisks.

Chart II



which enhance the resolution but reduce the signal to noise ratio.

Iron Chemical Shifts. Depending on the nature of the atoms bonded to iron in the complexes **1–28**, $\delta(^{57}\text{Fe})$ may vary by nearly 4000 ppm (Chart II). Within the $[(\eta^5\text{-Cp}')(\text{PR}_3)_2(\text{R})]\text{Fe}$ complexes an increasing electronegativity of the substituent at iron produces a lower shielding of the iron nucleus. Substitution at the organo residue R or at the $\eta^5\text{-Cp}'$ residue causes significantly smaller changes in the shielding of the metal nucleus. The iron shift can be assumed to be dominated by the paramagnetic shielding contribution,⁴⁰ which in a very rough approximation can be expressed by⁴¹ eq 1. In eq 1 $\langle r^{-3} \rangle$ denotes the mean radius

$$\delta(^{57}\text{Fe}) \sim \delta_{\text{para}} \sim \langle r^{-3} \rangle \sum_{\mu} P_{\mu} / \Delta E \quad (1)$$

of the valence d electrons, P_{μ} is the bond-order term, and ΔE is the average electronic excitation energy. The influence of the

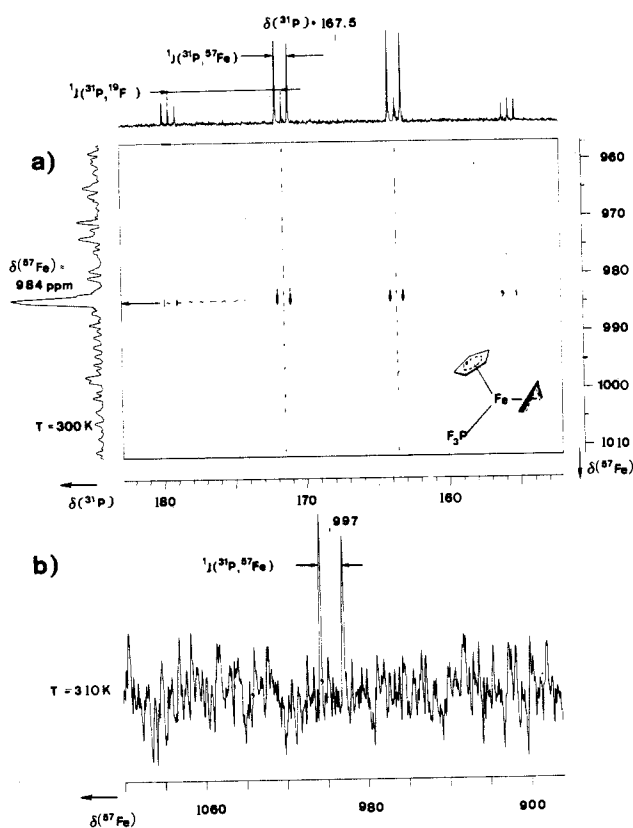


Figure 5. 12.9-MHz ^{57}Fe NMR spectra of $[(\eta^3\text{-allyl})(\eta^5\text{-Cp})\text{PF}_3]\text{Fe}$ (**30**). (a) An indirect ($^{31}\text{P}, \text{Fe}$) spectrum of a 5-mm sample tube is shown. Expansion of the range containing the cross peaks (here not illustrated) clearly shows that for **30** there is a (positive) $^2J(\text{F}, \text{Fe})$ coupling of about 3 Hz. (b) The $^{57}\text{Fe}\{^1\text{H}\}$ spectrum resulting from direct observation using a 10-mm sample tube is shown. Note that due to the higher temperature $\delta(^{57}\text{Fe})$ is higher in spectrum b. Due to the low sensitivity the $^2J(\text{F}, \text{Fe})$ coupling could not be resolved in the one-dimensional spectrum.

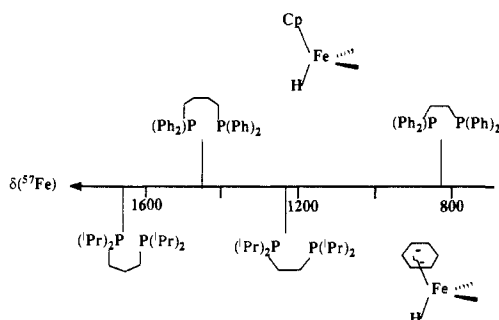
charge of the α -substituents upon $\delta(^{57}\text{Fe})$ can be rationalized by the $\langle r^{-3} \rangle$ dependence in eq 1. Substituents at phosphorus that affect the n -donor/ π -acceptor ability of the PR_3' ligands⁴² also cause significant changes of the iron chemical shifts. Strong π -acceptor ligands lead to an enhanced shielding of the iron nucleus. Within the $[(\eta^5\text{-Cp}')(\text{PR}_3)_2(\text{R})]\text{Fe}$ series, a change from $\text{P}(\text{OMe})_3$ (**25**) to PF_3 (**28**) causes the shielding of the metal nucleus to increase by about 1100 ppm. A difference of nearly half that amount is observed when $\delta(^{57}\text{Fe})$ of the monophosphane ($\eta^3\text{-allyl}$)Fe complexes **32** and **33** are compared with each other. This cannot be accounted for by the $\langle r^{-3} \rangle$ dependence of $\delta(^{57}\text{Fe})$. More probably, it is the $1/\Delta E$ dependence of $\delta(^{57}\text{Fe})$ that reflects the donor/acceptor ability of the phosphorus ligand. This hypothesis is substantiated by the results of cyclic voltammetry measurements,²⁸ which yield 0.22 and 1.0 V for the oxidation potentials of **25** and **28**, respectively. Thus, it can be assumed that the HOMO for complexes involving more basic ligands becomes higher. Consequently, for **25**, ΔE can be assumed to be smaller than for **28** and according to eq 1, $\delta(^{57}\text{Fe})$ should become larger, as is experimentally observed. This interpretation is supported by complexes of phosphanes with other organo residues. Upon substitution of phenyl groups by alkyl groups the phosphorus ligands become more basic⁴² and in line with the considerations made above, a higher shielding of the iron nucleus is observed (e.g. compare $\delta(^{57}\text{Fe})$ in **1–3**, in **22** and **23**, or in **13** and **16**). Furthermore, it must be noted that the replacement of both of the $\text{P}(\text{C}_6\text{H}_5)_2\text{Me}$ groups (**16**) by a chelating $(\text{C}_6\text{H}_5)_2\text{P}(\text{CH}_2)_2\text{P}(\text{C}_6\text{H}_5)_2$ ligand (**18**) produces a 600 ppm additional shielding of the iron nucleus. Apparently in complexes with bidentate ligands (e.g., **4**, **5**, **18**, or **24**), ΔE becomes larger, and a higher stability results. This is also indicated by the reaction conditions for ethylene

(40) Ramsey, N. F. *Phys. Rev.* **1950**, *78*, 699.

(41) Webb, G. A. In *NMR of Newly Accessible Nuclei*; Laszlo, P., Ed.; Academic: New York, 1983; Vol. 1, p 79 ff.

(42) Yarbrough, L. W.; Hall, M. B. *Inorg. Chem.* **1978**, *17*, 2269.

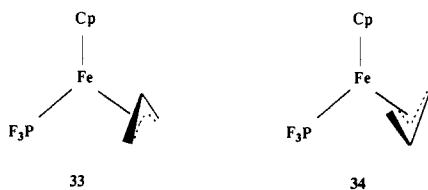
Chart III



insertion into the iron vinyl bond: whereas **22** and **23** add ethylene at $T = 40^\circ\text{C}$, **24** does not undergo an addition reaction until 160°C .²⁷

The iron shifts of complexes involving chelating phosphanes depend on the size of the iron-phosphorus-carbon ring (Chart III). The lowest $\delta(^{57}\text{Fe})$ values are observed when five-membered chelate rings are involved. Qualitatively similar chelate ring effects upon the metal shift have been found in molybdenum(0) complexes.⁴³ Again, the ^{57}Fe shifts resemble, at least in a qualitative manner, the thermal stability of the complexes. Whereas the $[(\eta^5\text{-Cp})(\text{R})]\text{Fe}$ complexes with five-membered bidentate ligands are stable against thermal decomposition until $T = 98^\circ\text{C}$, the corresponding complexes with seven-membered chelate rings decompose at temperatures below 50°C .

In the $[(\eta^3\text{-allyl})(\eta^5\text{-Cp}')\text{PR}_3]\text{Fe}$ series alkyl substitution at the allyl skeleton only produces small changes in $\delta(^{57}\text{Fe})$. The difference in $\delta(^{57}\text{Fe})$ between the exo and endo isomer of **33** and **34**



is 133 ppm. Here, the higher iron shielding belongs to the thermodynamically less stable isomer, indicating that the relation between the metal shielding and stability does not hold in every case. The iron shift difference however is larger than the difference between the $\delta(^{31}\text{P})$ values. The higher dispersion of the signals for the metal nuclei is advantageous for stereochemical studies and in particular when the isomers are in chemical exchange. Similar $\delta(^{57}\text{Fe})$ shift differences for stereoisomers of $[(\eta^3\text{-allyl})(\text{CO})_3\text{X}]\text{Fe}$ complexes were recently observed by Philipsborn.⁷

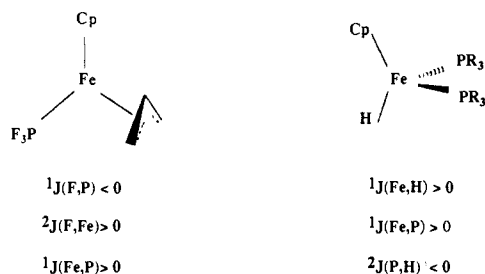
The chemical shift of the η^1, η^2 -alkenyl complexes **36–37** is in the same range as that observed for the complex $[(\eta^5\text{-Cp}^*)(\text{Me})(\text{PMe}_3)_2]\text{Fe}$ (**15**). Apparently substitution of the complexed ethylene by the PMe_3 ligand causes no significant change in the electronic environment of the iron nucleus. This interpretation is substantiated by the fact that the chemical shift of the $[(\eta^2\text{-ethylene})(\text{hydrido})]\text{iron}$ complex **38** is in the region one would expect for $[(\eta^5\text{-Cp}^*)(\text{H})(\text{PMe}_3)_2]\text{Fe}$.⁴⁴

Scalar Spin-Spin Coupling Constants $J(\text{Fe}, \text{X})$. In most of the $[(\text{L}_2)(\text{H})]\text{Fe}$ moieties mentioned here, the magnetically active nuclei ^{31}P , ^{57}Fe , and ^1H exhibit first-order spectra. Complexes **27** and **28**, however, yield second-order $\{\text{ABX}\}$ and $\{\text{AA}'\text{M}_3\text{M}_3'\text{X}\}$ spectra ($\text{A}, \text{B} = ^{31}\text{P}; \text{M} = ^{19}\text{F}, \text{X} = ^{57}\text{Fe}$). For these complexes, spectral parameters were obtained by analysis of the F_2 projection of the corresponding indirect two-dimensional spectrum (cf. Figure 3). Identical $J(\text{P}, \text{P})$ and $J(\text{P}, \text{F})$ values were obtained by analysis of the conventional one-dimensional $162\text{-MHz } ^{31}\text{P}\{^1\text{H}\}$ spectrum. Therefore, it can be assumed that the F_2 projection of the indirect

(43) Alyea, E. C.; Somogyvari, A. *Magn. Reson. Chem.* **1985**, *24*, 357.

(44) Comparison of $\delta(^{57}\text{Fe})$ in **13** and **15** indicates that going from $(\eta^5\text{-Cp})$ to $(\eta^5\text{-Me}_5\text{-Cp})$ causes a deshielding of the iron nucleus of about 300 ppm. Therefore, $\delta(^{57}\text{Fe})$ in $[(\eta^5\text{-Cp}^*)(\text{hydrido})(\text{PMe}_3)_2]\text{Fe}$ is expected to lie around 1600 ppm.

Chart IV

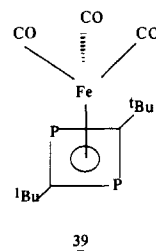


two-dimensional double-quantum spectrum yields reliable NMR parameters by standard spectral analysis as long as the coupling is not strong (in **27** $(\delta_A - \delta_{AB})/J_{AB}$ is about 3 at 9.4 T). It must be noted, however, that for **27** and **28** in the two-dimensional contour plots the internal F_1 projection does not yield the correct splitting of the X part of the corresponding spectrum. Similar effects have also been observed in the INEPT and DEPT spectra of silver complexes.⁴⁵ We attribute this fact to the higher order of the spin systems in **27** and **28**.⁴⁶

The data in Tables II–V demonstrate that $^1J(\text{Fe}, \text{P})$ may become relatively large. Conventional wisdom tells one that the scalar iron-phosphorus coupling constants are dominated by the Fermi contact term in eq 2 where $|\text{S}(\text{O})|^2$ denotes the s electron density

$$J(\text{Fe}, \text{P}) \sim \gamma_{\text{Fe}}\gamma_{\text{P}}|\text{S}(\text{O})|_{\text{Fe}}^2|\text{S}(\text{O})|_{\text{P}}^2\pi\pi_{\text{Fe}, \text{P}} \quad (2)$$

at the nucleus and $\pi_{\text{Fe}, \text{P}}$ stands for the mutual polarizability.⁴⁷ In the phosphorus compounds listed in Tables II–V, the largest $^1J(\text{Fe}, \text{P})$ values are found when there are highly electronegative substituents attached to phosphorus (i.e. when the ligand has the highest π -acceptor power). Compare $^1J(\text{Fe}, \text{P})$ in **29**, **35**, **31**, and **33**. This can be rationalized by a contraction of the phosphorus orbitals, which leads to an increase of the electron density at phosphorus and, therefore, according to eq 2 to larger $^1J(\text{Fe}, \text{P})$ values. Such effects have previously been reported for $^1J(\text{M}, \text{P})$ in $\text{Ni}(\text{PR}_3)_4$ ⁴⁸ and $(\text{CO})_5\text{WPR}_3$ ⁴⁹ complexes.⁵⁰ In line with this interpretation is the observation that $J(\text{Fe}, \text{P})$ couplings involving π -bonds are relatively small. In diphosphaferrocenes $^1J(\text{Fe}, \text{P})$ was found to be around 16 Hz,⁷ and in the (diphosphacyclobutadiene)iron complex **39**, $^1J(\text{Fe}, \text{P})$ is 10 Hz.⁵¹



In the hydridoiron complexes **1–15** and **38** the $^1J(\text{Fe}, \text{H})$ values do not vary significantly upon the substitution of other ligands at the iron. A similar situation holds for the $^2J(\text{Fe}, \text{F})$ values in

(45) Bernes Price, S. J.; Brevard, C.; Pagelot, A.; Sadler, P. J. *Inorg. Chem.* **1985**, *24*, 4278.

(46) A detailed study describing how indirectly recorded two-dimensional spectra due to sequences 1–3 (cf. Figure 1) are affected by spin systems of higher order is in progress.

(47) Webb, G. A. In *NMR and the Periodic Table*; Harris, R. K., Mann, B. E., Eds.; Academic: New York, 1978; p 67.

(48) Hao, N.; McGlinchey, M. J.; Sayer, B. G.; Schrobilgen, G. J. *J. Magn. Reson.* **1982**, *46*, 158.

(49) Head, R. A.; Nixon, J. F.; Sharp, G. J.; Clark, R. J. *J. Chem. Soc., Dalton Trans.* **1975**, 2054.

(50) Verkade, J. G.; Mosbo, J. A. In *Methods in Stereochemical Analysis*; Verkade, J. G., Quin, L. D., Eds.; Weinheim, FRG, Verlag Chemie: 1987; Vol. 8, p 425f.

(51) Benn, R.; Ruffińska, A., unpublished results. ($\delta(^{57}\text{Fe})$ of **39** is -557 .) For a recent review dealing with the synthesis of diphosphacyclobutadiene transition-metal complexes, cf.: Binger, P.; Milczarek, P.; Mynott, R.; Krüger, C.; Tsay, Y.-H.; Raabe, E.; Regitz, M. *Chem. Ber.* **1988**, *121*, 637.

complexes **28**, **38**, **33**, and **34**. Since the sign of $^1J(\text{P},\text{F})$ in these metal complexes can be assumed to be negative⁵² from the two-dimensional correlation experiments (cf. Figure 4b), it follows that $^2J(\text{F},\text{Fe})$ is positive. Of particular value is the combination of two-dimensional experiments, e.g. ($^1\text{H},^{57}\text{Fe}$) and ($^{31}\text{P},^{57}\text{Fe}$) for complex **1**. In this way, the relative signs of a variety of scalar couplings in quasitrigonal and -tetragonal complexes can be obtained (cf. Chart IV). To the best of our knowledge, the signs

of $J(\text{Fe},\text{X})$ couplings have not hitherto been reported.

Registry No. **1**, 84283-30-7; **2**, 110118-63-3; **3**, 110118-62-2; **4**, 51509-20-7; **5**, 115161-07-4; **6**, 97959-87-0; **7**, 115161-08-5; **8**, 115161-09-6; **9**, 115161-10-9; **10**, 115161-11-0; **11**, 115161-12-1; **12**, 78192-57-1; **13**, 78192-62-8; **14**, 110118-41-7; **15**, 94585-62-3; **16**, 110118-38-2; **17**, 115161-13-2; **18**, 51509-19-4; **19**, 110118-44-0; **20**, 110118-48-4; **21**, 115161-14-3; **22**, 110118-53-1; **23**, 110118-52-0; **24**, 97959-85-8; **25**, 115161-15-4; **26**, 115161-16-5; **27**, 115161-17-6; **28**, 115161-18-7; **29**, 115161-19-8; **30**, 115161-20-1; **31**, 115161-21-2; **32**, 115161-24-5; **33**, 115161-22-3; **34**, 115224-90-3; **35**, 115161-23-4; **36**, 110118-78-0; **37**, 110118-82-6; **38**, 94585-64-5.

(52) Staplin, D. C.; Parry, R. W. *Inorg. Chem.* **1979**, *18*, 1473.

Observation of Molecular Reorientation in Ice by Proton and Deuterium Magnetic Resonance

R. J. Wittebort,^{*,†} M. G. Usha,[†] D. J. Ruben,[‡] D. E. Wemmer,[§] and A. Pines[§]

Contribution from the Department of Chemistry, University of Louisville, Louisville, Kentucky 40292, Francis Bitter National Magnet Laboratory, Massachusetts Institute of Technology, Cambridge, Massachusetts 02139, and Department of Chemistry, University of California, Berkeley, Berkeley, California 94720. Received December 31, 1987

Abstract: We have directly observed molecular reorientation in polycrystalline hexagonal ice, ice I_h , by deuterium NMR and deuterium-decoupled proton NMR. The dynamics are seen as exchange broadening of powder patterns. The reorientational rates required to produce similar effects on the patterns are scaled according to the magnitudes of the anisotropic spin interactions, ~ 6 kHz for the proton-shielding anisotropy or ~ 200 kHz for the deuterium quadrupolar coupling in water. Because of the differing sizes of these two interactions, the two methods are complementary for studying reorientation over the temperature range 200–267 K. The results show that water molecules reorient with tetrahedral symmetry in ice. Line-shape simulations using the assumption of tetrahedral reorientation are in accord with the experimental spectra and give rates directly comparable to the temperature-dependent Debye correlation time, τ_D , from dielectric relaxation.

We report here the direct observation by deuterium and proton magnetic resonance of tetrahedral jump motions in normal hexagonal ice I_h . This result returns one to Pauling's 1935 observation that, in ice I_h , where each oxygen is tetrahedrally surrounded by four half-hydrogens, there is no single hydrogen-bonding configuration for the crystal.¹ Thus, the orientation of each molecule is not uniquely specified. With the attendant combinatorial consequences, Pauling accurately estimated the known² residual entropy as $Nk_B \ln(3/2)$. Improvements in Pauling's calculation³ and a neutron diffraction structure directly showing the disorder in the deuteron positions of hexagonal D_2O^4 have confirmed the correctness of the original idea. The question then arises as to whether or not ice molecules can interconvert among the different crystal configurations and, if so, at what rate and by what molecular mechanism(s). Ice has a measurable conductivity and a substantial polarizability (large ϵ_0), suggesting that different configurations could be generated by proton transfer and by molecular rotation. The rate question has been addressed by studying the effects of electric field jumps on conductivity⁵ and by measurements of dielectric relaxation.^{6,7} In the latter, the characteristic Debye correlation time, $\tau_D \sim 10^{-5}$ s at about 263 K, is related in some way to dipole moment reorientation resulting either from proton transfer or molecular rotation. Auty and Cole⁶ declined to interpret their dielectric relaxation experiments in terms of either of these possibilities but noted that the relaxation process is characterized by a single relaxation time and a large activation energy, $E_A = 13.5$ kcal/mol, or about 3 times the hydrogen-bond energy. Bjerrum⁸ addressed the matter of how water molecules

reorient in ice without violating the Bernal-Fowler rules for hydrogen bonding. He assumed that a small concentration of orientational defects, so-called D (two hydrogens between oxygens) and L defects (no hydrogens between oxygens), naturally occur. Once a defect is formed, neighboring waters are then relatively free to rotate with consequent relocation of the defect, but without creating additional H-bonding mismatches in the lattice. Eisenberg and Kauzman, in their standard monograph,⁹ assumed the dielectric relaxation to arise from reorientation and, on the basis of theoretical considerations, approximately equated the rotational correlation time with the dielectric correlation time; i.e., $\tau_c \sim \tau_D$. This connection thus suggests that a water molecule, at a temperature just below the freezing point, experiences $\sim 10^5$ reorientations/s. Gränicher et al. have argued, however, that in ice interconversion among the $(3/2)^N$ configurations does not occur by molecular rotation.⁷

The methods used here^{10,11} directly detect molecular reorientation by exchange modulation of the deuteron quadrupolar

- (1) Pauling, L. *J. Am. Chem. Soc.* **1935**, *57*, 2680.
- (2) Giaque, W. F.; Ashley, M. *Phys. Rev.* **1933**, *43*, 81.
- (3) Nagle, J. F. *J. Math. Phys. (Cambridge, Mass.)* **1966**, *7*, 1484.
- (4) Peterson, S. W.; Levy, H. A. *Acta Crystallogr.* **1957**, *10*, 70.
- (5) Eigen, M. *Angew. Chem., Int. Ed. Engl.* **1964**, *3*, 1.
- (6) Auty, R. P.; Cole, R. H. *J. Chem. Phys.* **1952**, *20*, 1309.
- (7) Gränicher, H.; Jaccard, C.; Scherrer, P.; Steinemann, A. *Discuss. Faraday Soc.* **1958**, *23*, 50.
- (8) Bjerrum, N. *Science (Washington, D.C.)* **1951**, *115*, 385.
- (9) Eisenberg, D.; Kauzman, W. *The Structure and Properties of Water*; Oxford University: Oxford, 1969.
- (10) Wemmer, D. E. Report LBL-8042; University of California, Berkeley; Berkeley, CA, 1978.
- (11) Wittebort, R. J.; Woehler, S. E.; Bradley, C. A. *J. Magn. Reson.* **1986**, *67*, 143.

[†]University of Louisville.

[‡]Massachusetts Institute of Technology.

[§]University of California, Berkeley.